This is a repository copy of *Self-assembly of amphiphilic statistical copolymers and their aqueous rheological properties*.

White Rose Research Online URL for this paper:
http://eprints.whiterose.ac.uk/126797/

Version: Accepted Version

eprints@whiterose.ac.uk
https://eprints.whiterose.ac.uk/

Self-assembly of amphiphilic statistical copolymers and their aqueous rheological properties

Thomas J. Neal,[a] Deborah L. Beattie,[a] Sarah J. Byard,[a] Gregory N. Smith,[a] Martin W. Murray,[b] Neal S. J. Williams,[b] Simon N. Emmett,[b] Steven P. Armes,[a] Sebastian G. Spain,*[a] Oleksandr O. Mykhaylyk*[a]

[a] Department of Chemistry, Dainton Building, The University of Sheffield, Sheffield, S3 7HF, UK.

[b] AkzoNobel Decorative Paints, Wexham Road, Slough, Berkshire, SL2 5DS, UK

ABSTRACT. A range of poly(n-butyl methacrylate-stat-methacrylic acid) [P(BMA-stat-MAA)] statistical copolymers of various compositions and molecular weights ranging from 5 to 30 kDa were prepared using either reversible addition-fragmentation chain transfer (RAFT) solution copolymerization or conventional free radical polymerization in isopropanol (IPA). On dilution with water, these amphiphilic copolymers self-assembled to form spherical nano-objects as confirmed by small-angle X-ray scattering (SAXS) and transmission electron microscopy. Various structural particle models were examined to extract information regarding the mean nano-object size and morphology. It is found that nano-object radii are independent of copolymer molecular weight, but depend on the copolymer composition: the smaller the amount of MAA units in the molecules the larger the nano-objects are formed. Combined SAXS and aqueous electrophoretic measurements indicated that most of the MAA units are located at the nano-object surface. Furthermore, SAXS and rheology measurements were used to monitor the effect of solvent composition on the copolymer morphology both at a fixed copolymer concentration (either 1 wt% or 25 wt%) and also for a gradual variation in copolymer

concentrations (from 1 wt% to 40 wt%) when adding water to the initial copolymer solution in IPA. These studies revealed that the copolymers are present in solution as molecularly-dissolved Gaussian chains when the solvent composition is IPA-rich. However, the copolymer chains self-assemble into spherical nano-objects when the solvent composition is water-rich. At intermediate solvent compositions, SAXS analysis confirmed the formation of an interconnected nano-object network, which accounts for the apparently anomalous increase in solution viscosity on dilution indicated by rheology measurements.

INTRODUCTION. Amphiphilic copolymers are used in various applications including drug delivery, cosmetics, paints, and coatings.[1,2] They comprise both hydrophilic and hydrophobic monomers and are known to self-assemble in aqueous solution to form a wide range of nanoscale morphologies.[3] The self-assembly of diblock copolymers has been extensively studied as they can produce well-defined morphologies, such as spheres,[4–12] worms[13] or vesicles,[14,15] which can often be predicted by their molecular parameters such as the chemical nature of each comonomer and the mean degree of polymerization (DP) of each block.[16] In comparison, the nanostructures formed by amphiphilic statistical copolymers are relatively under-studied. Nevertheless, both spherical nano-objects and other morphologies have been reported depending on the hydrophilic/hydrophobic balance.[17–21]

Chang and McCormick demonstrated how the distribution of a hydrophobe along the backbone of a statistical copolymer affected its self-assembly.[22] Statistical copolymers prepared *via* conventional free radical polymerization (FRP), had a tendency to undergo intramolecular hydrophobic interactions. In contrast, copolymers containing micro-domains (short blocks) of the hydrophobe displayed intermolecular association that was enhanced by the size of these micro-domains. This association behaviour was further investigated by studying the effects of incorporating various bulky hydrophobic substituents, such as lauryl (LA), cyclodecyl (CD), and 1-adamantyl (AD) methacrylamides into the copolymer chain.[23] Copolymers containing bulkier CD and AD substituents more strongly favoured intramolecular association compared with the LA-based copolymer. Moreover, reducing the number of

hydrophobic groups significantly reduced both the aggregation number and the particle radius.[23] More recently, Sato *et al.* investigated how the composition and the degree of polymerization affected the aqueous micellization behavior of a series of amphiphilic statistical copolymers synthesized *via* reversible addition-fragmentation chain transfer (RAFT) polymerization.[23] The results from this study indicated a strong influence of the mean DP and copolymer composition on the aggregation number and the number of hydrophobic micro-domains per aggregate, with higher DPs leading to lower aggregation number. Sato *et al.*, further analyzed the self-assembly of statistical copolymers by investigating the effect of varying both the hydrophobic and ionic comonomer units on the micellar structure.[24] Like Kamachi *et al.*[2] higher hydrophobic monomer contents led to larger aggregation numbers (and hence particle size). Furthermore, varying the type of ionic monomer had little effect on the micellar structure.[24]

As well as spherical nano-objects, other relatively unusual copolymer assemblies, such as giant vesicles, honeycomb films and bowl-shaped aggregates, have been achieved through the aggregation of amphiphilic statistical copolymers.[25–30] An example of one of these higher-order architectures was reported by Lui and Zhu in 2011, who demonstrated that vesicles could be formed by the self-assembly of L-glutamic acid-based amphiphilic random copolymers in an ethanol/water mixture.[25] Structures such as honeycomb films and spheres were also achieved using evaporative self-assembly from various solvents, including dichloromethane and methanol.

Although the self-assembly of amphiphilic statistical copolymers has been investigated to some extent, there is only a rather limited understanding of how such behavior can affect the physical properties of such dispersions. Although this question has been overlooked, it is essential when evaluating these systems for commercial applications. Furthermore, there have been only limited studies of such systems using scattering techniques combined with detailed structural analysis and modelling.[31] Herein an extensive study is conducted to assess the effect of composition, molecular weight, concentration and solvent composition on the self-assembly of a series of anionic amphiphilic statistical copolymers in *iso*-propanol/water solution and the resulting physical properties of such colloidal dispersions. More

specifically, a series of methacrylic statistical copolymers were synthesised *via* RAFT copolymerization in order to achieve a wide range of comonomer compositions and narrow molecular weight distributions. Additionally, a series of similar copolymers were synthesized *via* conventional free radical copolymerization to examine the effect of dispersity (M_w/M_n) on copolymer self-assembly. The micellar structures formed by these amphiphilic copolymers were characterized by small-angle X-ray scattering (SAXS) in dilute solution in order to evaluate their morphology. A series of structural models have been developed to analyze the resulting SAXS patterns. Finally SAXS studies were also conducted at higher copolymer concentrations to account for the anomalous rheological behaviour of such dispersions, which leads to an increase in solution viscosity on dilution with water.

EXPERIMENTAL SECTION.

Materials. Butyl methacrylate (BMA, 99%), and methacrylic acid (MAA, 99.5%) were purchased from Sigma-Aldrich (Gillingham, UK) and were passed through basic alumina to remove inhibitors prior to use. Isopropanol (IPA, 99.9%), triethanolamine (TEA, 99%), glacial acetic acid (99.85%), 4,4'-azobis(4-cyanovaleric acid) (ACVA, 98%), trimethylsiyl diazomethane solution (2.0 M in diethyl ether) and deuterated acetone were purchased from Sigma-Aldrich and used as received unless stated otherwise in the text. High-performance liquid chromatography grade tetrahydrofuran (THF) and deuterated chloroform were purchased from VWR (Lutterworth, UK). Deionised water was obtained using an Elgastat Option 3A water purifier. 4-cyano-4-(2-phenyl-ethanesulfanylthiocarbonyl) sufanylpentanoic acid (PETTC) was prepared in-house as reported previously.[32]

Gel permeation chromatography (GPC). The molecular weight distributions were determined by GPC using THF containing 1 wt% acetic acid and 0.054 w/v% butyl hydroxytoluene (BHT) as the eluent. Separations were performed using a pair of Plgel Mixed-C columns (7.8 × 300 mm, 5 μm bead size) at a flow rate of 1.0 mL min⁻¹. The GPC system was equipped with a WellChrom K-2301

refractive index detector measuring at wavelength 950 ± 30 nm. All the samples were measured relative to a set of ten near-monodisperse poly(methyl methacrylate) (PMMA) standards with peak molecular weight values ranging from 1,280 to 330,000 Da.

SAXS measurements. SAXS patterns were collected using laboratory SAXS instruments, either Bruker AXS Nanostar modified with Xenocs GeniX 3D system designed for CuK_α radiation (wavelength $\lambda = 1.54$ Å), two sets of motorized collimating scatterless slits and equipped with a 2D Hi-STAR multi-wire gas detector or a Xenocs Xuess 2.0 laboratory beamline equipped with a Dectris Pilatus 1M detector and an Excillum liquid gallium MetalJet X-ray source ($\lambda = 1.34$ Å). The majority of the patterns were collected over a scattering vector range of 0.008 Å^{-1} to 0.16 Å^{-1}. The length of the scattering vector, q, is given by $q = (4\pi / \lambda)\sin\theta$, where θ is half the scattering angle. X-ray scattering data reduced by Nika SAS macros for Igor Pro (integration, normalisation, background subtraction)[33] were further analysed using Irena SAS macros for Igor Pro.[34] Scattering of water was used for absolute intensity calibration of SAXS patterns.

Aqueous Electrophoresis. The electrophoretic mobility of aqueous copolymer dispersions, with an electrolyte background of 0.75 mM KCl, was measured using phase-analysis light scattering (PALS) on a Malvern Zetasizer Nano ZS instrument.

¹H NMR spectroscopy. ^{1}H NMR spectra were recorded on either a Bruker AV1-400 or AV3HD-400 MHz spectrometer in either CDCl$_3$ or (CD$_3$)$_2$CO. Typically, 64 scans were averaged per spectrum. Spectra were analyzed with Bruker Topspin 3.0 software and the chemical shifts are reported in ppm relative to the residual solvent peak. In order to calculate the copolymer composition, the copolymer methacrylic acid units were methylated to methyl methacrylate using trimethylsiyldiazomethane (TMS-DAM) prior to the NMR measurements as previously reported.[35]

Transmission electron microscopy (TEM). TEM studies were conducted using a Philips CM 100 instrument operating at 100 kV and equipped with a Gatan 1k CCD camera. Copper/palladium TEM grids (Agar Scientific, UK) were coated with a thin layer of carbon and then glow discharged for 30 seconds. Samples were prepared by placing a droplet (10 μL) of diluted copolymer dispersions (0.1 % w/w) to the carbon-coated copper grids for 1 minute. Once the excess dispersion was removed by dabbing the grids with filter paper uranyl formate (9.0 μL of a 0.75% w/w solution) was placed on the grids for 20 seconds and then dabbed with filter paper. Each sample was additionally dried using a vacuum hose.

Rheology. An MCR 502 rheometer (Anton Paar, Gratz, Austria) equipped with a TruGap system for automatic gap control and configured for cone-and-plate geometry (50 mm diameter, angle 2°) with a solvent trap was used for measuring dynamic viscosity of the copolymer dispersions at various concentrations and solvent compositions. In order to reduce any shear-induced change in copolymer morphology, an oscillatory mode was chosen for the measurements. Preliminary strain sweep experiments, between 0.1% and 20% strain at constant angular frequencies were performed for all copolymer samples to identify the linear viscoelastic region. Once a suitable strain had been identified, an angular frequency sweep, downwards from 200 rad s^{-1} to 0.1 rad s^{-1}, was conducted at a constant strain (typically 1%) and temperature (21 °C) to measure the dynamic viscosity (Figure S1). The dynamic viscosity determined for each copolymer dispersion displayed almost no frequency dependence at frequencies below 10 rad s^{-1}. Thus, this region of rheological data was used to obtain zero shear viscosity defined by an extrapolation of the experimental results to zero angular frequency. Such obtained values of zero shear viscosity were used for the characterization of copolymer dispersions.

RESULTS AND DISCUSSION.

Synthesis of BMA/MAA Amphiphilic Copolymers. A series of twelve poly(*n*-butyl methacrylate-*stat*-methacrylic acid) [P(BMA-*stat*-MAA)] copolymers was synthesized with varying comonomer compositions and molecular weights *via* RAFT solution copolymerization (Figure 1). PETTC and ACVA were used as the chain transfer agent (CTA) and initiator, respectively, and the CTA/initiator molar ratio was maintained at 5.0. RAFT chemistry was used to ensure narrow molecular weight distributions and good control over the target copolymer molecular weight. The twelve copolymers were purified by precipitation from solution into a 1:1 ratio of water/methanol mixture to remove any residual comonomers. The purified copolymers were isolated as white/yellow powders. The lower molecular weight copolymers were more yellow owing to their higher proportion of RAFT chain-ends. GPC analysis showed that the copolymer molecular weight ranged from 6.1 kDa to 22.3 kDa with M_w/M_n values always below 1.25 (Table 1).
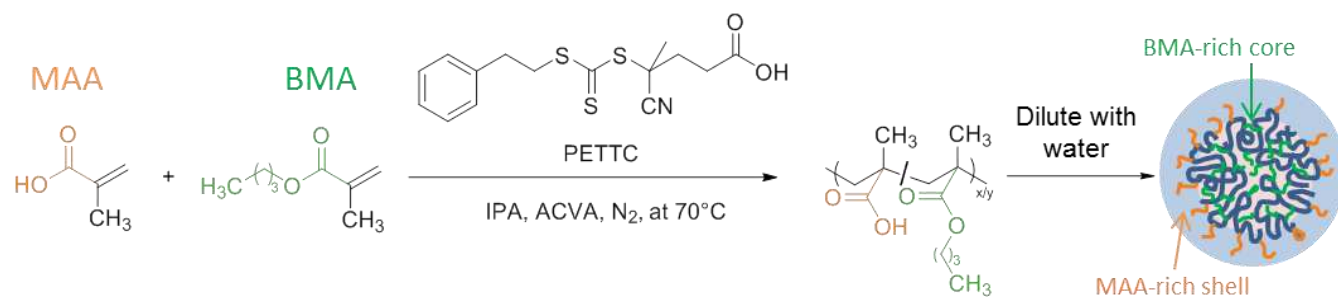

Figure 1. Synthesis of amphiphilic P(BMA-*stat*-MAA) statistical copolymers by RAFT solution copolymerization using a PETTC RAFT agent and an ACVA initiator followed by micellar self-assembly on addition of water.

BMA and MAA comonomers were added into the reaction solution at molar feed ratios of 70:30, 80:20, and 90:10, respectively (Table S1). Determination of the copolymer compositions using ^{1}H NMR spectroscopy indicated that there were fewer MAA units present in the copolymer than expected from the initial feed ratio (Table 1). Intantaneous comonomer conversions were determined throughout the

polymerization by ^{1}H NMR spectroscopy (Figure S2) and comparable initial rates of polymerization were obtained for each comonomer ($k_{obs} \approx 0.0028$ s^{-1}) which should lead to statistical incorporation. However, after 430 minutes the reaction rate of MAA decreases significantly ($k_{obs} \approx 0.0001$ s^{-1}), resulting in a substantially lower MAA conversion compared to that of BMA (63 mol % vs. 93 mol %, respectively). It is not known why the observed MAA conversion is limited but such kinetic data does clarify why the MAA content of the final copolymers is always less than that targeted. Taking the lower ultimate MAA conversion into account, the theoretical BMA/MAA copolymer compositions can be recalculated as 77:23, 85:15, and 93:7, which is in good agreement with compositions determined from ^{1}H NMR analysis of the methylated copolymers. However, because the BMA comonomer continues to polymerize after MAA polymerization has essentially stopped, this produces a short BMA-rich 'blocky' sequence at the end of each copolymer chain.

Table 1. Compositional data obtained from ^{1}H NMR analysis of methylated copolymers [P(BMA-stat-MMA)], weight-average molecular weight (M_w) and dispersity (M_w/M_n) obtained by GPC analysis of P(BMA-*stat*-MAA) copolymers using a THF eluent containing 1.0 wt% acetic acid (AcOH).

Synthesis	Label	NMR		THF + 1 wt% AcOH GPC	
		BMA content	MMA content	M_w, kDa	M_w/M_n
RAFT	BM$_{77:23(22k)}$	0.79	0.21	21.9	1.25
	BM$_{77:23(15k)}$	0.76	0.24	13.1	1.20
	BM$_{77:23(10k)}$	0.80	0.2	11.2	1.19
	BM$_{77:23(5k)}$	0.78	0.22	6.1	1.20
	BM$_{85:15(22k)}$	0.87	0.13	22.3	1.24
	BM$_{85:15(15k)}$	0.85	0.15	11.4	1.19
	BM$_{85:15(10k)}$	0.88	0.12	8.6	1.19
	BM$_{85:15(5k)}$	0.84	0.16	6.6	1.19
	BM$_{93:7(22k)}$	0.94	0.06	22.3	1.23
	BM$_{93:7(15k)}$	0.93	0.07	12.5	1.16
	BM$_{93:7(10k)}$	0.93	0.07	10.6	1.16

	BM$_{93:7(5k)}$	0.92	0.08	7.0	1.16
FRP	FRP$_{70:30(24k)}$	0.69	0.31	23.9	1.81
	FRP$_{80:20(31k)}$	0.78	0.22	31.2	1.89
	FRP$_{90:10(21k)}$	0.88	0.12	21.2	1.85

An additional series of P(BMA-*stat*-MAA) copolymers was synthesized by monomer-starved conventional free radical solution copolymerization in IPA. This protocol should produce copolymer molecules with evenly distributed BMA and MAA units along the chain, which enables a comparison to be made to the potentially less even monomer distribution in the copolymers prepared by RAFT copolymerization. Again, copolymer compositions of 70:30, 80:20 and 90:10 were targeted by varying the BMA/MAA comonomer feed ratios. These target compositions were fully consistent with ^{1}H NMR analysis of the methylated copolymers (Table 1). These copolymers have significantly higher dispersities ($M_w/M_n \approx 1.85$) than those synthesized via RAFT copolymerization ($M_w/M_n \approx 1.20$). Thus, the latter technique provides better control over the molecular weight distribution (Table 1).[36]

Copolymer Self-assembling in Water. The self-assembly behavior of these amphiphilic copolymers in water was investigated using SAXS. To avoid formation of large copolymer aggregates, dispersions were prepared using IPA as a co-solvent. Furthermore, TEA (1.1 mol. equivalents to the MAA residues) was added to the copolymer dispersions to deprotonate the MAA units and hence increase their water solubility. Thus, copolymers were first dissolved at 50 wt% in IPA and deprotonated with TEA before dilution to 1.0 wt% with water. This protocol yielded colloidally stable dispersions/solutions for most formulations. However, attempts to prepare copolymer dispersions at high copolymer concentrations with low IPA contents (indicated in Figure S3) were unsuccessful, owing to aggregation and precipitation.

SAXS patterns recorded for 1.0 wt% copolymer dispersions in water showed features consistent with the formation of particles with a clearly defined Guinier region at $q < 0.04$ Å^{-1} and the first minimum of

the form factor at $q \sim 0.08$ Å^{-1} (Figures 2 and 3). Analysis of these scattering patterns was undertaken by attempting to fit the data using appropriate structural models.

In general, the intensity of the X-rays scattered by a dispersion of similar particles can be expressed *via* the differential scattering cross-section per unit sample volume, $d\Sigma/d\Omega(q)$, which is defined as the product of the particle form factor and the structure factor:

$$\frac{d\Sigma}{d\Omega}(q) = NS(q) \int_0^\infty \dots \int_0^\infty F(q, r_1, \dots, r_k) \Psi(r_1, \dots, r_k) dr_1 \dots dr_k \quad (1),$$

where $F(q, r_1, \dots, r_k)$ is the form factor defined by a k number of r parameters, $\Psi(r_1, \dots, r_k)$ is the distribution function of these parameters, N is the number density per unit volume and $S(q)$ is the structure factor.

The copolymers under investigation comprise either a fully statistical or a predominantly statistical distribution of BMA and MAA units. Thus, according to the literature, such copolymers should form approximately spherical nano-objects (or, for the sake of simplicity, particles).[17,18] However, since there is no diblock copolymer architecture, it can be assumed that phase separation between the hydrophobic and hydrophilic units is negligible. Therefore, no well-defined core and corona domains are expected for these self-assembled morphologies. This means that a spherical form factor should be appropriate to describe these nano-objects:

$$F_s(q, r_1) = N_{agg}^2(r_1) \beta_s^2 A_s^2(q, r_1) \quad (2),$$

where r_1 is the nano-object radius, $A_s(q, r_1)$ is the sphere form factor amplitude defined as:

$$A_s(q, r_1) = \frac{3[\sin(q, r_1) - qr_1 \cos(q, r_1)]}{(qr_1)^3} \quad (3)$$

and the mean nano-object aggregation number $N_{agg}(r_1)$ is expressed as:

$$N_{agg}(r_1) = (1 - x_{sol}) \frac{4\pi r_1}{3V_s} \quad (4),$$

where x_{sol} is the volume fraction of solvent within the nano-object. The scattering length contrast of the nano-object described by eq 4 is given by $\beta_s = V_s(\xi_s - \xi_{sol})$, where ξ_s and ξ_{sol} represent the scattering

length densities of the copolymer and background solvent, respectively. ξ_s in this case represents the averaged scattering length density of the copolymer, which is calculated as:

$$\xi_s = \xi_{BMA} \cdot v_{BMA} + \xi_{MAA} \cdot v_{MAA} \quad (5),$$

where v represents the respective volume fractions of BMA and MAA repeat units in the copolymer, and ξ_{BMA} and ξ_{MAA} are the respective scattering length densities of PBMA (9.80×10^{10} cm^{-2}) and PMAA (10.70×10^{10} cm^{-2}). The ξ_{sol} was calculated from the scattering length densities and volume fractions of the solvent components. In particular, in this work mixtures of water ($\xi_{H2O} = 9.42 \times 10^{10}$ cm^{-2}) and IPA ($\xi_{C3H8O} = 7.55 \times 10^{10}$ cm^{-2}) were used in this analysis. The total volume of an average copolymer molecule, V_s, is obtained as a sum of the average volumes of both the BMA and MAA components in the copolymers calculated using the equation $V_{BMA\ or\ MAA} = M_w/(N_A\rho_{BMA\ or\ MAA})$, where M_w is the product of the number of BMA or MAA repeat units per chain and the BMA or MAA repeat unit mass. The solid-state densities of the homopolymers, $\rho_{PBMA\ or\ PMAA}$, were determined by helium pycnometry [$\rho_{PBMA} = 1.05$ g cm^{-3} and $\rho_{PMAA} = 1.18$ g cm^{-3}].

The polydispersity of the nano-object radius, expressed as a Gaussian distribution, is considered for the structural model (eq 1):

$$\Psi(r_1) = \frac{1}{\sqrt{2\pi\sigma_{Rs}^2}} e^{-\frac{(r_1 - R_s)^2}{2\sigma_{Rs}^2}} \quad (6),$$

where R_s is the mean nano-object radius and σ_{Rs} is its standard deviation. The number density per unit volume (eq 1) is expressed as:

$$N = \frac{\phi}{\int_0^\infty V(r_1)\Psi(r_1)dr_1} \quad (7),$$

where ϕ is the total volume fraction of copolymer molecules in the sample and $V(r_1)$ is the total *volume* of copolymer chains within the nano-object [$V(r_1) = V_s N_{agg}(r_1)$].

It is commonly accepted that the Percus-Yevick approximation is suitable for describing structural peaks originating from particle interactions at high concentrations (at or above 5 vol%).[37] However, a

pronounced peak of intensity at $q \sim 0.02$ Å^{-1} was observed consistently in the scattering patterns even at copolymer concentrations as low as 1.0 wt% owing to long-range repulsive interactions between the anionic nano-objects (Figures 2 and 3). Indeed, addition of a small amount of NaCl results in the loss of this feature (Figure S4). Thus, two structure factors were evaluated within the SAXS model (eq 1) to account for this additional feature. The first is based on the Percus-Yevick approximation,[37,38] $S(q) = S_{PY}(q, R_{PY}, f_{PY})$, where R_{PY} is an interparticle correlation radius and f_{PY} is an effective volume fraction, and second is based on the Hayter-Penfold approximation for charged particle Coulomb interactions,[39] $S(q) = S_{HP}(q, R_{HP}, f_{HP}, M, T, \varepsilon, Q)$, where R_{HP} is an interparticle correlation radius, f_{HP} is an effective volume fraction, M is the ionic strength of the solvent, T is the absolute temperature, ε is the solvent dielectric constant and Q is the particle charge expressed in electrons.

The particle charge required for the Hayter-Penfold approximation could be calculated from the electrophoretic mobility (μ_e) of the P(BMA-*stat*-MAA) particles as determined by aqueous electrophoresis. Mobility can be converted into a ζ-potentials using the Henry equation:[40]

$$\mu_e = \frac{2}{3} \frac{\varepsilon_{rs}\varepsilon_0}{\eta_w} \zeta f(\kappa R_s) \quad (8),$$

where ε_{rs} is the dielectric constant of water, ε_0 is the permittivity of vacuum, η_w is the dynamic viscosity of water, κ is the inverse Debye length and $f(\kappa R_s)$ can be obtained from the Oshima expression.[40] The apparent charge (Q) can be related to the effective ζ-potential by solving the linearized Poisson-Boltzmann equation:[41]

$$Q = \frac{R_s(1+\kappa R_s)}{\lambda_B} \frac{e\zeta}{k_B T} \quad (9),$$

where λ_B is the Bjerrum length,[41] and k_B is the Boltzmann constant. The aggregation observed for MAA-rich copolymer nano-objects means that their electrophoretic mobility value is less reliable than for well-dispersed nano-objects. Nonetheless, there is a clear correlation between the particle radius and the

particle surface charge (Table S2). From these measurements, an average charge was calculated for the copolymer compositions and used in the Hayter-Penfold approximation (Table 2).

The proposed model (eqs 1 and 2) should demonstrate a strong power law dependence at high q [$d\Sigma/d\Omega(q) \sim q^{-4}$]. However, the experimental SAXS data (Figures 2 and 3) indicate a relatively flat curve in this q range ($q > 0.1$ Å^{-1}), especially for the pattern corresponding to $BM_{93:7(22k)}$ (Figure 3b). This type of behavior is commonly observed for diblock copolymer micelles owing to scattering from the corona blocks.[42] For random copolymers, this is an unexpected result. Nevertheless, randomly-packed MAA and BMA residues within the nano-objects may well produce regions with differing scattering length densities. Such fluctuations in scattering length density within the nano-objects should cause scattering at high q. Similar structural formation has been analyzed using a 'blob' model.[43] This approach was developed to interpret neutron scattering from the solvated cores of spherical micelles, where the Debye function for a Gaussian polymer chain[44]

$$F_{chain}(x) = 2[\exp(-x) - 1 + x]/x^2 \quad (10),$$

where $x = (qR_g)^2$ and R_g is the radius of gyration of the copolymer chains, was used in the analytical form factor calculations of the scattering length density fluctuations described as independent blobs.

Thus, this "blob" model[43] was incorporated into the structural model describing the form factor of nano-objects formed by statistical copolymers:

$$F_{sb}(q, r_1) = N_{agg}^2(r_1)\beta_s^2 \left[n_{blob}(n_{blob} - 1)\psi^2(qR_g^{blob})A_s^2(q, r_1) + n_{blob}F_{chain}(qR_g^{blob}) \right] /$$

$$n_{blob}^2 \quad (11),$$

where $\psi(y) = [1 - \exp(-y)]/y$, $y = (qR_g^{blob})^2$ is the form factor amplitude of a 'blob' (polymer chain), R_g^{blob} is the 'blob' radius of gyration and $F_{chain}(qR_g^{blob})$ is the self-correlation term of the Gaussian polymer chain ('blob') represented by the Debye function (eq 10). $n_{blob} = A_1V_{obj}/V_{blob}$ is an

approximate number of 'blobs', where A_1 is a fitting parameter, $V_{obj} = 4/3\pi r_1^3$ and $V_{blob} = 4/3\pi(R_g^{blob})^3$.

The approach produced a reasonably good fit to the experimental SAXS data (Figure 2, black line). However, a reliable set of 'blob' parameters could not be obtained from data fits owing to relatively noisy data at high q. Thus, although some fittings returned physically reasonable values (for example, $R_g^{blob} \approx 4$ Å, and $n_{blob} \approx 0.07$) suggesting that the average 'blob' size might correspond to approximately two repeat units, this 'blob' model was replaced with a simplified approach. Since it is associated with a minor component of the copolymer chains, the characteristic 'blob' size should be relatively small. Hence any function describing the 'blob' scattering (e.g., a Debye function) should be more or less constant within the studied q range. Thus, the model chosen for SAXS data analysis was

$$\frac{d\Sigma}{d\Omega}(q) = NS(q) \int_0^\infty F_s(q, r_1)\Psi(r_1)dr_1 + C_1 \; (12),$$

where the constant C_1 is a fitting parameter that is independent of q and represents the flat background produced by the scattering length density fluctuations across the nano-object.
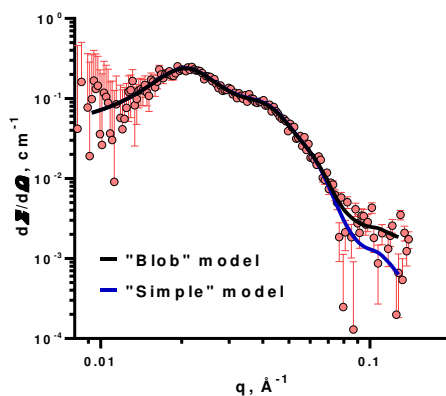

Figure 2. SAXS pattern recorded for a 1.0 wt% aqueous dispersion of $BM_{85:15(22k)}$ (symbols) fitted with both the 'blob' model (eqs 3 and 12; black line) and the simple sphere model (eqs 3-5; blue line). A Bruker AXS Nanostar instrument was used for these measurements.

The proposed model produced reasonably good fits to the scattering patterns obtained for 1.0 wt% P(BMA-*stat*- MAA) copolymer aqueous dispersions (Figure 3), yielding the nano-object radii for each system (Table 2). However, SAXS patterns for the $BM_{77:23}$ samples displayed some upturn at low q (Figure 3b), suggesting the presence of large aggregates. A combination of Guinier and power law functions is commonly employed to describe the scattering from large randomly-shaped structures.[45,46,47] However, the Guinier region located at very low q is often inaccessible in SAXS experiments and only the power law region is recorded in scattering patterns. Thus, in order to fit the upturn in intensity observed in the scattering patterns, an additional term describing the power law dependence at low q was incorporated into the model:[45,46,47]

$$\frac{d\Sigma}{d\Omega}(q) = NS(q)\int_{0}^{\infty} F_s(q, r_1)\Psi(r_1)dr_1 + C_1 + B \cdot q^{-P} \quad (13)$$

where B is a prefactor that depends on the type of power-law scattering, as determined by the regime in which P falls. For example, for $P = 4$ this power law dependence corresponds to Porod's law and B is the Porod constant. The refined model was used for SAXS analysis and a least-squares algorithm was employed for data fits. However, a genetic optimization algorithm was applied when the global minimum of the figure of merit for the fitting ("chi-squared" parameter) had to be identified, in some cases, particularly for the model utilizing the Hayter-Penfold structure factor.

When fitting experimental SAXS patterns using eq 13, the two structure factor approximations produced different values for the structural parameters describing particle packing in these copolymer dispersions (Table 2). More specifically, the interparticle distances and effective volume fractions obtained using the Percus-Yevick approximation were systematically larger than those values calculated when employing the Hayter-Penfold approximation. Nevertheless, the form factor parameters (FF column in Table 2) were not influenced by the chosen structure factor functions and employing either Percus-Yevick or Hayter-Penfold approximation produced very similar results for the particle radius, which was the most important parameter for this study. In view of this finding, the less parameterized Percus-Yevick approximation was used for SAXS analysis in the rest of this work.

Considering eq 13 in combination with eqs 2, 4 and 7 suggests that ϕ and x_{sol} are positively covariant. Thus, when the above model was used for data fitting, the volume fraction was fixed at the known concentration of the copolymer dispersion in order to evaluate x_{sol}. This approach yielded x_{sol} values close to zero, suggesting minimal ingress of the water molecules within the P(BMA-*stat*-MAA) nano-objects.

Table 2. Summary of SAXS analyses of a series 1.0 wt% P(BMA-*stat*-MAA) copolymer nano-objects in aqueous media: mean particle radius (R_s), standard deviation of the mean particle radius (σ_{Rs}) and mean aggregation number (N_{agg}) calculated from the form factor function (FF), and the interparticle correlation distance (R_{HP} or R_{PY}), the effective volume fraction (f_{HP} or f_{PY}) and particle charge (Q) obtained using the Hayter-Penfold (HP) and Percus-Yevick (PY) structure factors, respectively.

	FF			HP*			PY	
Sample	R_s, Å	σ_{Rs}, Å	N_{agg}	R_{HP}, Å	Q, electrons	f_{HP}	R_{PY}, Å	f_{PY}
BM$_{77:23(22k)}$	37	7	6	70	20	0.05	113	0.13
BM$_{77:23(15k)}$	33	6	7	61	20	0.05	100	0.12
BM$_{77:23(10k)}$	34	7	9	54	20	0.03	96	0.12
BM$_{77:23(5k)}$	37	5	22	65	20	0.05	85	0.10
BM$_{85:15(22k)}$	51	9	16	114	30	0.14	144	0.23
BM$_{85:15(15k)}$	49	7	28	91	30	0.08	139	0.20
BM$_{85:15(10k)}$	53	8	47	116	30	0.11	156	0.19
BM$_{85:15(5k)}$	54	7	64	92	30	0.05	156	0.18
BM$_{93:07(22k)}$	85	11	74	-	67	-	230	0.19
BM$_{93:07(15k)}$	81	19	114	-	67	-	284	0.15
BM$_{93:07(10k)}$	66	12	73	-	67	-	220	0.20
BM$_{93:07(5k)}$	68	17	120	-	67	-	233	0.17
FRP$_{70:30(24k)}$	35	13	5	47	20	0.05	77	0.15
FRP$_{80:20(31k)}$	66	16	25	97	30	0.04	176	0.16
†FRP$_{90:10(21k)}$	137	33	281	-	-	-	-	-

*No reliable results could be obtained for the BM$_{93:07}$ copolymers using the HP structure factor

†No structural peak was observed in the FRP$_{90:10(21k)}$ scattering pattern

SAXS analysis indicates a correlation between the copolymer composition and the mean nano-object radius, with MAA-rich copolymers producing smaller nano-objects (Table 2). In contrast, the copolymer molecular weight has rather little effect on the nano-object size, particularly for the 77:23 and the 85:15 compositions. The anionic MAA groups stabilize the nano-objects and higher MAA contents lead to lower mean aggregation numbers. Analysis of the 93:7 copolymer series indicates that the nano-object radius increases for the two higher molecular weights (Table 2). This suggests that the RAFT chain-ends help to solubilize the lower molecular weight copolymers: using PETTC as the CTA produces copolymer chains with an ionizable carboxylic acid end-group, which behaves like an additional MAA group. For relatively low MAA contents and copolymer molecular weights, such as $BM_{93:7(10k)}$ or $BM_{93:7(5k)}$, these end-groups effectively increase the carboxylic acid content of these MAA-based and, as a result, smaller nano-object radii are formed. Thus, higher molecular weight copolymers (15 kDa or 22 kDa) are more representative of the 93:7 composition.

Since there is no consistent correlation between copolymer molecular weight and nano-object size, the dispersity should have relatively little effect. Indeed, similar analysis undertaken on the FRP-synthesized copolymer series demonstrates a comparable trend, whereby the MAA composition is inversely related to the nano-object dimensions (Table 2). Although the compositional dependence is similar for the two synthesis methods, some discrepancies can be identified when a direct comparison between RAFT- and FRP- synthesized copolymers is made. Generally, the nano-objects formed by the FRP series tend to be larger than those formed by the RAFT series as the MAA content is lowered. This size difference could be the result of statistical variations in the distribution of MAA units along the copolymer chains, as indicated by the BMA/MAA copolymerization rate (Figure S2), as well as the incorporation of an additional carboxylic acid group per chain for the RAFT-synthesized copolymers.

TEM images obtained after drying 0.1 wt% copolymer dispersions confirm the formation of spherical nano-objects (Figure 4) and are consistent with the SAXS data. Moreover, TEM analysis also suggests that MAA-rich copolymers form smaller nano-objects. However, SAXS is considered far more

statistically robust than TEM, with the latter technique also prone to staining artefacts and the possibility of nano-object flattening occurring during drying.
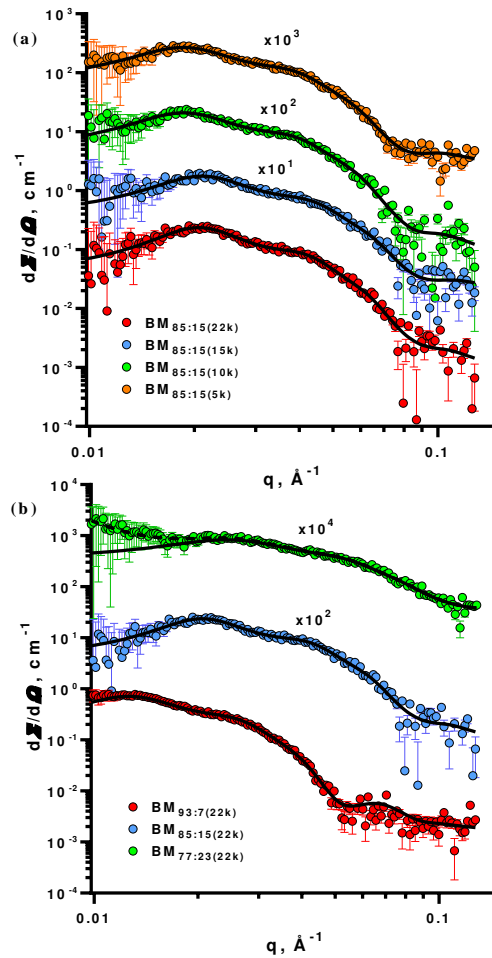

Figure 3. SAXS patterns recorder for 1.0 wt% aqueous dispersions of P(BMA-stat-MAA) copolymer nano-objects (symbols) fitted using a refined spherical particle model (eq 13, solid lines) and (eq 14, dashed line); where (a) compares the scattering from a series of copolymers of the same composition (BM$_{85:15}$) but differing molecular weights and (b) compares the scattering for copolymers of the same molecular weight (22 kDa) but differing copolymer compositions. A Bruker AXS Nanostar instrument was used for these measurements. Some patterns are shifted upward by arbitrary factors (as indicated on the plots) to avoid overlap.
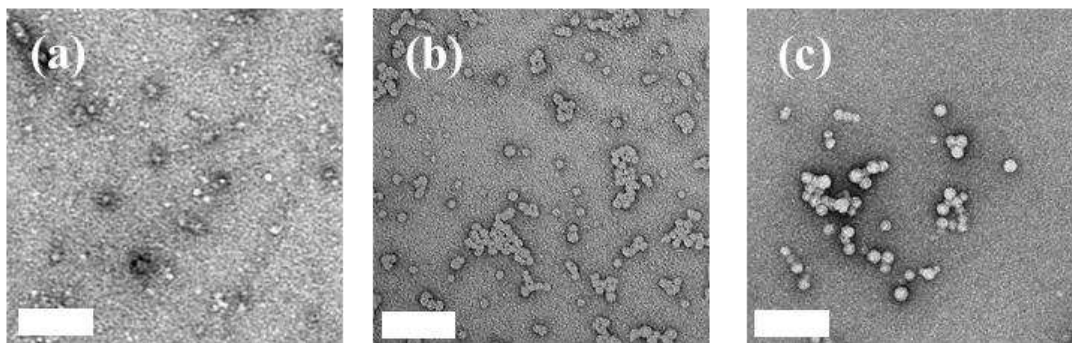
Figure 4. TEM images recorded for P(BMA-*stat*-MAA) spherical nano-objects formed after dilution to 0.1 wt% with water from an initial 50 wt% copolymer solution in IPA for: (a) BM$_{77:23(22k)}$; (b) BM$_{85:15(22k)}$; and (c) BM$_{93:7(22k)}$. The white scale bar in each TEM image corresponds to 100 nm.

Effect of varying the IPA/water solvent composition at a fixed copolymer concentration. The colloidal stability of the spherical nano-objects was examined by increasing the IPA content of the solvent mixture. More specifically, a series of SAXS measurements were conducted on 1.0 wt% copolymer dispersions with differing IPA/water contents (Figure 5a). Firstly, the structure factor observed of 1.0 wt% aqueous copolymer dispersions disappears on addition of IPA, indicating that the long range order arising from the mutually repulsive anionic nano-objects is lost. This is a result of a reduction in the dielectric constant for the IPA/water mixture, and thus an increase in pKa,[48] reducing the effective anionic charge density on the surface of the nano-objects. Furthermore, larger, more solvated (i.e. higher x_{sol}) nano-objects are formed as the IPA content is increased (Figure 5a). The scattering pattern recorded when the IPA volume fraction is 0.43 shows an upturn in scattering intensity at $q < 0.02$ Å^{-1}, suggesting the formation of significantly larger nano-objects. In pure IPA, there is no self-assembly because IPA is a sufficiently good solvent to fully solubilize the copolymer chains. A similar experiment was conducted using a 25 wt% copolymer dispersion (Figure 5b). In this case, well separated spherical nano-objects are formed when the binary solvent is water-rich, as indicated by the pronounced structure factor peak observed under these conditions. However, as the solvent environment

becomes IPA-rich, this feature becomes less prominent suggesting a reduction in nano-object size and an increase in the mean interparticle distance. A slight upturn at low q is evident at an IPA volume fraction of 0.31, which suggests the formation of larger nano-objects. At IPA volume fractions above 0.43, the structure factor peak is no longer observed (Figure 5b), which indicates molecular dissolution of individual copolymer chains under these conditions.
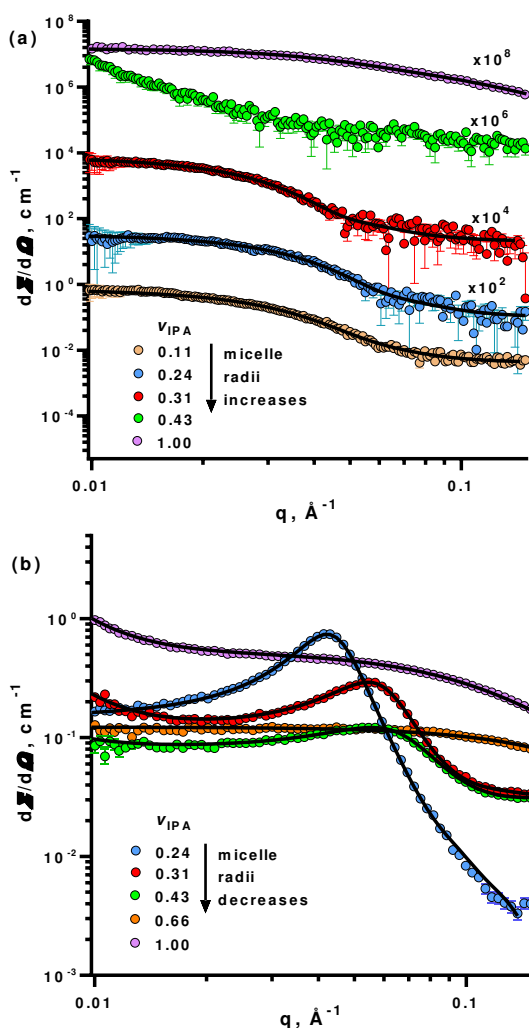

Figure 5. (a) SAXS patterns recorded for 1.0 wt% $BM_{85:15(22k)}$ copolymer dispersions (symbols) where the solvent composition is varied from water-rich to IPA-rich (a Bruker AXS Nanostar instrument was used for these measurements), with some patterns shifted upward by an arbitrary factor (indicated on the plots) to avoid overlap; (b) SAXS patterns recorded for 25 wt% $BM_{85:15(22k)}$ copolymer dispersions where the solvent composition is varied from water-rich to IPA-rich (a Xenocs Xeuss

instrument was used for these measurements). The IPA/water solvent composition is indicated by the IPA volume fraction, v_{IPA}. SAXS data are fitted to an adapted spherical particle model (eq 13, solid lines).

These SAXS studies confirm that these P(BMA-*stat*-MAA) copolymers are mainly present as molecularly-dissolved Gaussian chains in IPA-rich media, whereas micellar self-assembly occurs at high water volume fractions owing to the hydrophobic nature of the BMA residues. This is true for both high (25 wt%) and low (1.0 wt%) copolymer concentrations. Under the latter conditions, the spherical nano-objects become swollen in IPA and hence grow in size when the solvent composition is gradually changed from water-rich to IPA-rich. In contrast, the particles appear to *decrease* in size when performing the same solvent switch at 25 wt% copolymer. This observation is accompanied by a scattering intensity upturn at low q-values suggesting the formation of larger objects.

Clearly, the extent of self-assembly is affected by both the solvent composition and the copolymer concentration. However, it is also important to compare the above two data sets to understand why different trends are observed. At 1.0 wt%, the nano-objects are well-separated, which enables them to swell unhindered on IPA addition, as confirmed by SAXS (Figure 5a). However, at 25 wt% copolymer, the particles are much closer together and the IPA-swollen nano-objects interpenetrate to form a copolymer network interconnected by relatively small nano-object cores. This structural arrangement produces large scattering objects, resulting in a discernible upturn in scattered intensity at low q (Figure 5b). Thus, SAXS patterns of the dilute copolymer dispersion correspond to a system comprising large, large, non-interacting nano-objects composed of solvated coronas and non-solvated cores. In contrast, the scattering patterns obtained for the corresponding concentrated dispersion of interpenetrating nano-objects are consistent with smaller non-solvated nano-object cores embedded within a homogeneous matrix comprising highly solvated copolymer chains and solvent. Hence the apparent size reduction observed at higher IPA concentrations for concentrated dispersions is associated with an effective reduction in volume of the particle cores.

Effect of varying both the copolymer concentration and the solvent composition. To further investigate the effect of copolymer concentration on nano-object self-assembly, SAXS studies were conducted on 10, 20, 25, and 30 wt% copolymer dispersions in IPA-rich solvent compositions (Figure 6). Simultaneous variation of the copolymer concentration and solvent compositions enables a wide range of sample compositions to be examined by performing relatively few experiments. A structure factor peak was observed in the scattering patterns these studies were conducted at high copolymer concentrations, for which of IPA solvation of the BMA segments is less significant (Figure 6). This feature shifts to higher q at higher copolymer concentrations, indicating a shorter interparticle distance and hence more densely-packed nano-objects (Figure 6). Moreover, it becomes less pronounced at higher copolymer and IPA concentrations. This trend is particularly evident for $BM_{77:23(22k)}$ – its structure factor is barely discernible at 30 wt% copolymer. In contrast, the more moderate change in the structure factor peak associated with $BM_{93:7(22k)}$ series of samples indicates a correlation between particle stability and copolymer composition: BMA-rich copolymer nano-objects are less likely to undergo dissociation under these conditions.
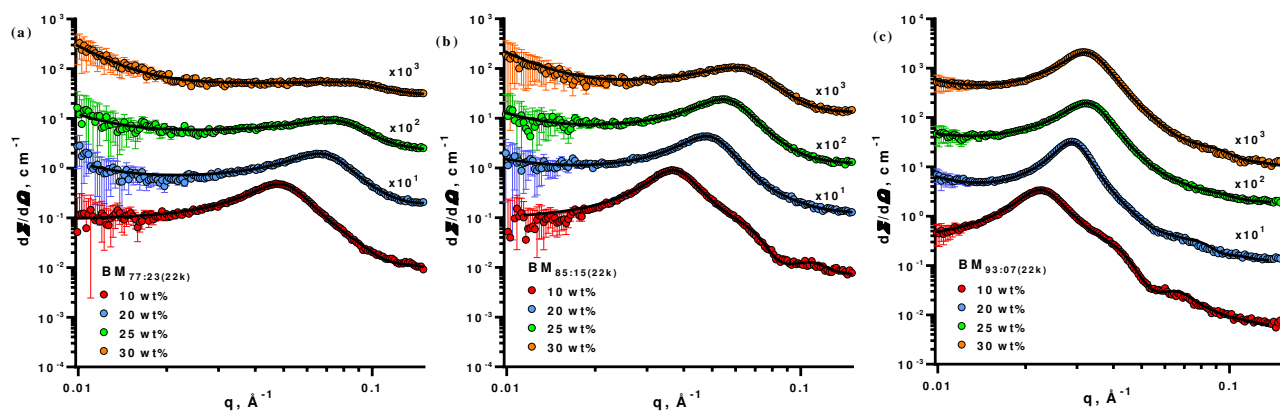

Figure 6. SAXS patterns recorded at 10, 20, 25 and 30 wt% copolymer dispersions (see symbols) for (a) $BM_{77:23(22k)}$, (b) $BM_{85:15(22k)}$ and (c) $BM_{93:7(22k)}$ in various IPA/water solvent mixtures (the IPA volume fraction, v_{IPA}, is 0.11, 0.24, 0.31 and 0.43, respectively). A Bruker AXS Nanostar instrument

22

was used for these measurements. Some patterns are shifted upward by an arbitrary factor indicated on the plots to avoid overlap. The SAXS data are fitted using an adapted spherical nano-object model (eq 13, solid lines).

The spherical nano-objects formed at 10 wt% copolymer concentration are of a similar size to that determined at 1.0 wt% but the relative interparticle distance is significantly reduced, as expected at this higher copolymer concentration (compare Tables 2 and 3). The observed reduction in nano-object dimensions when increasing the copolymer concentration (Table 3) is attributed to the higher IPA content in the binary solvent mixture. This is consistent with the observed increase in the solvent volume fraction within the nano-objects (x_{sol}) obtained from SAXS analysis (eq 4). Thus, the nano-object size and mean aggregation number are reduced in IPA-rich media. The shift and attenuation in the structure factor peak observed in these scattering patterns, despite the higher copolymer concentration, suggests a morphological transformation from spherical nano-objects at low copolymer concentration in water-rich media towards molecularly-dissolved copolymer chains in IPA-rich media. As expected, this trend is most noticeable for MAA-rich copolymers (Figure 6a). At 30 wt% copolymer, the nano-objects possess their smallest dimensions and are highly swollen. Indeed, x_{sol} is close to unity, which seems to be physically unrealistic. The model assumes the sole presence of spherical nano-objects and that all the copolymer chains are located within the nano-objects. Since the copolymer volume fraction is fixed during data fitting, such high x_{sol} values suggest that the fitting algorithm artificially lowers the nano-object scattering contribution by reducing the (1 - x_{sol}) term in eq 6. A reasonable explanation is that not all copolymer chains are located within the nano-objects. Given that IPA is a reasonably good solvent for the BMA residues and that the structural morphology is less defined at high copolymer concentrations and IPA volume fractions, the single population of spherical nano-objects assumed in this scattering model is an over-simplified approximation. Indeed, given the broad distribution of copolymer compositions, BMA-rich chains are more likely to form nano-objects, whereas MAA-rich chains are more likely to be molecularly dissolved. Thus, these two populations may well coexist,

particularly at higher IPA volume fractions. In this case the SAXS pattern can be represented by a superposition of scattering contributions from both nano-objects (eq 2) and random coils (eq 10) where the total copolymer concentration, redistributed between these two populations, is fixed. However, this refined two-population model does not provide a satisfactory fit to the experimental data at high q. An alternative model involves a single population of nano-objects whereby some of the copolymer chains form bridges between neighboring nano-objects to produce an extended network (Figure 7). In this case the copolymer volume fraction located within the nano-objects and, therefore, the total nano-object volume will be reduced. At the same time, the interconnected nano-objects form a larger network of objects that scatter coherently. Indeed, the relevant SAXS patterns exhibit a gradual upturn in scattering at low q values (Figure 6) with the scattering intensity following a power law dependence (with an exponent of ~ -3 at the highest IPA content, see Figures 6a and 6b) that suggests the formation of large fractals. However, the Guinier region for these structures could not be resolved at low q (~ 0.002 Å^{-1}), which suggests that their dimensions exceed 3000 Å. In general, these SAXS observations support the formation of a nano-object network interconnected by partially released copolymer chains (Figure 7). Satisfactory qualitative fits to scattering patterns can be obtained using a relatively simple structural model (eq 13) incorporating a spherical micelle form factor (eq 2) (Figure 6). However, quantitative SAXS analysis of this inter-connected nano-object network is beyond the scope of this work. In addition, redistribution of solvent molecules is likely for IPA-rich dispersions, since this co-solvent can readily penetrate the nano-objects. Such variation of the solvent composition inside and outside the nano-objects and concomitant reduction in the scattering length density contrast between IPA-swollen nano-objects and the binary solvent mixture may account for the artificially high x_{sol} suggested by the data fits.

SAXS analysis suggests that the self-assembled morphology transforms from well-defined nano-objects to interconnected nano-objects to molecularly-dissolved copolymers (Figure 7). At low copolymer concentrations in a water-rich environment, the copolymer chains self-assemble to form stable nano-objects. However, increasing the copolymer concentration along with the IPA volume

fraction causes a reduction in nano-object size and formation of an interconnected nano-object network. At the highest IPA volume fractions, the copolymer chains become fully solvated and undergo molecular dissolution.
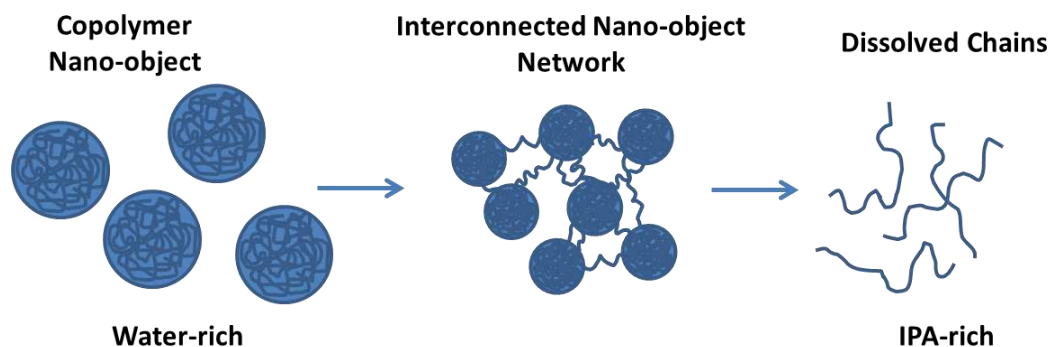

Figure 7. A schematic describing the transformation from self-assembled copolymer nano-objects (at low copolymer concentrations in a water-rich environment) to dissolved chains (at high copolymer concentrations in an IPA-rich environment) via an interconnected nano-object network.

Table 3. Summary of the structural parameters obtained from SAXS studies of a three series of amphiphilic P(BMA-*stat*-MAA) statistical copolymers [$BM_{77:22(22k)}$, $BM_{85:15(22k)}$, and $BM_{93:7(22k)}$] dissolved at various concentrations in IPA-water solutions using a refined model (eq 13) comprising a spherical form factor (FF) and Percus-Yevick structure factor (PY): mean nano-object radius (R_s), solvent fraction in the nano-objects (x_{sol}), the interparticle correlation radius (R_{PY}) and effective volume fraction (f_{PY}).

Polymer	wt%	Solvent content		FF		PY	
		v_{IPA}	v_{Water}	R_s, Å	x_{sol}	R_{PY}, Å	f_{PY}
BM$_{77:23(22k)}$	10	0.11	0.89	41	0.39	62	0.30
	20	0.24	0.76	32	0.84	44	0.28
	25	0.31	0.69	25	0.93	37	0.23
	30	0.43	0.57	17	0.97	30	0.21
BM$_{85:15(22k)}$	10	0.11	0.89	52	0.45	85	0.34
	20	0.24	0.76	45	0.85	63	0.32
	25	0.31	0.69	39	0.92	54	0.30
	30	0.43	0.57	33	0.97	45	0.24
BM$_{93:7(22k)}$	10	0.11	0.89	84	0.46	139	0.35
	20	0.24	0.76	80	0.82	112	0.40
	25	0.31	0.69	69	0.88	95	0.35
	30	0.43	0.57	68	0.92	96	0.35

Rheology of copolymer dispersions. Rheological studies were performed on the same copolymer dispersions of various concentrations and solvent composition to determine their dynamic viscosity and to monitor any physical consequences of the structural phenomena detected by SAXS (Figures 5, 6, and 7). Initial experiments were conducted on 25 wt% copolymer dispersions with the binary solvent composition being varied from IPA-rich to water-rich (Figure 8) to assess how this parameter affects their rheological behavior. When the solvent environment is IPA-rich (i.e., when the volume fraction of IPA, v_{IPA}, is at least 0.66) a relatively low viscosity is observed (Figure 8), which is attributed to the molecularly-dissolved copolymer chains (Figure 5b and Figure 7). However, when the water content is increased ($0.43 \geq v_{IPA} \geq 0.31$), the copolymer chains self-assemble to form interconnected nano-objects (Figure 5b and Figure 7). This nano-object network leads to a sharp increase in the dispersion viscosity (Figure 8), indicating a significant reduction in chain mobility. When the solvent environment is water-rich ($v_{IPA} \leq 0.24$) the copolymers form well-defined spherical nano-objects (Figure 5b and Figure 7) leading to a significant reduction in the dispersion viscosity (Figure 8), as expected for isolated particles in a Newtonian liquid[49]. An extended series of viscosity measurements on BM$_{85:15(22k)}$ performed over a wider range of copolymer concentrations and solvent compositions indicates the local maximum in zero

shear viscosity (Figure S3). These data confirms that both a high copolymer concentration and a higher proportion of IPA co-solvent are required for the formation of a nano-object network.
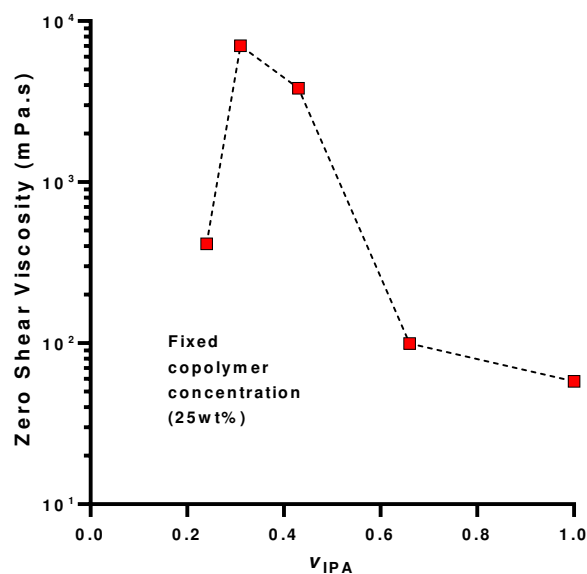

Figure 8. Zero shear viscosity observed for 25 wt% $BM_{85:15(22k)}$ copolymer dispersions containing various volume fractions of IPA co-solvent (v_{IPA}).

In order to compare various P(BMA-*stat*-MAA) copolymers, rheological measurements were conducted for copolymer concentrations ranging from 1.0 to 40 wt% (Figure 9). Formulations were selected with appropriate copolymer concentration and v_{IPA} to correspond approximately with the diagonal line crossing the local maximum of zero shear viscosity (Figure S3). These studies were combined with the SAXS data (Figure 6 and Table 3) in order to evaluate the effect of self-assembly on the copolymer dispersion viscosity.

Dilute copolymer dispersions (1.0 wt%) and water-rich solvent compositions exhibited zero shear viscosities (Figure 9) comparable with that of water (~ 1 mPa.s). These observations are consistent with the corresponding SAXS data (Figure 3), which indicate the formation of spherical nano-objects under these conditions. Such weakly repulsive anionic copolymer nano-objects (as indicated by combined

electrophoresis and SAXS studies) do not significantly affect the rheological properties of the dispersion. Indeed, rheology measurements performed at copolymer concentrations up to 20 wt% indicate relatively low dispersion viscosities of 20-100 mPa.s (Figure 9b). The viscosity trend at 20 wt% copolymer concentration appears to be inversely correlated to the nano-object size, where the dispersions with larger sphere radii displaying lower viscosities.
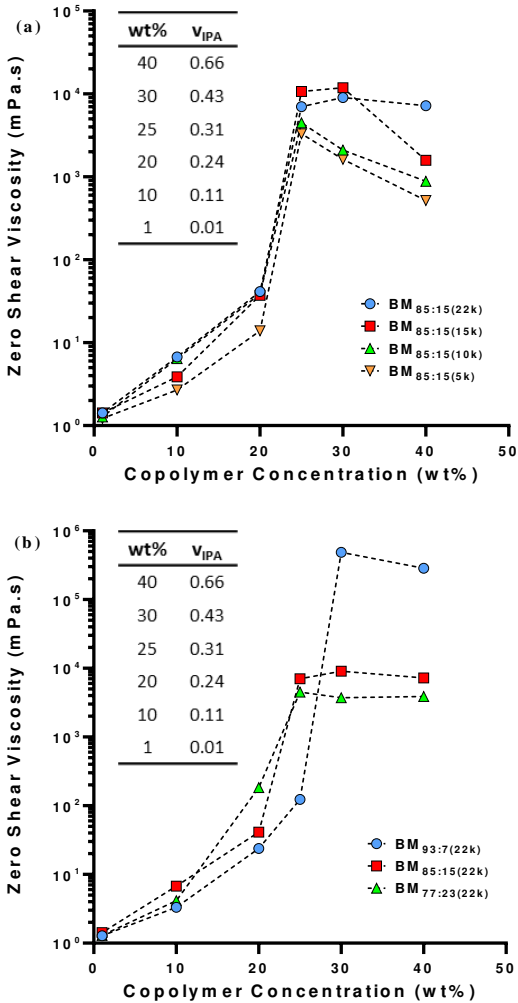

Figure 9. Zero shear viscosity *versus* copolymer concentration for P(BMA-*stat*-MAA) dispersions diluted from a 50 wt% copolymer stock solution in IPA with water: (a) copolymer dispersions of the same copolymer composition but differing molecular weights (BM$_{85:15(22k)}$, BM$_{85:15(15k)}$, BM$_{85:15(10k)}$, and BM$_{85:15(5k)}$); (b) copolymer dispersions of the same molecular weight but differing copolymer

composition [$BM_{77:23(22k)}$, $BM_{85:15(22k)}$, and $BM_{93:7(22k)}$]. The table in each plot shows the composition of the studied samples (copolymer concentrations and respective IPA volume fraction in the solvent).

Each copolymer displays a local maximum in viscosity at concentrations ranging from 25 wt% to 30 wt%. For example, the copolymer series containing the highest MAA content (Figure 9b) displays a sharp increase in viscosity at the lowest copolymer concentration (25 wt%) and v_{IPA} (0.31). This correlates well with the SAXS data (Figure 6a), which suggests that $BM_{77:23(22k)}$ copolymers no longer form well-defined spherical nano-objects at this concentration but instead form an interconnected nano-object network, as indicated by the scattering intensity upturn at low q. Furthermore, rheology measurements show that BMA-rich copolymers (Figure 9b) display a viscosity maximum at the highest concentration of 30 wt% where the v_{IPA} is 0.43. Again, this observation is consistent with the SAXS data (Figure 6c), which shows that $BM_{93:7(22k)}$ copolymers at this concentration form a nano-object network at this concentration.

Further inspecting the rheology data indicates a strong relationship between the maximum viscosity and the copolymer composition. The former parameter increases with lower MAA contents, consequently there is a correlation between the maximum viscosity and the nano-object radius. At 40 wt% copolymer, the IPA content in the copolymer dispersions becomes significant, which promotes molecular dissolution. Moreover, the viscosity depends on the copolymer molecular weight such that the longest chains produce the most viscous solutions (Figure 9a). This is consistent with the SAXS data and suggests that the copolymer chains are molecularly dissolved at this concentration. Furthermore, the viscosity of 40 wt% copolymer solution not only depends on the molecular weight but also on the copolymer composition, with the highest viscosity being achieved for the lowest MAA fraction (Figure 9b). An extended set of viscosity measurements using a wider range of copolymer concentrations and solvent compositions to further map out the peak in viscosity (Figure S3).

Overall, there is a good correlation between the copolymer morphologies determined by SAXS and viscoelastic properties of the copolymer dispersions: well-defined spherical nano-objects behave as a

Newtonian liquid,[49] interconnected nano-object networks are characterized by an increase in dispersion viscosity by more than two orders of viscosity compared to well separated nano-objects, while molecularly-dissolved copolymer chains exhibit the rheological behavior expected for a polymer solution.

The relationship between nano-objects size and the copolymer composition. According to the SAXS data the nano-objects size is strongly dependent on the copolymer composition. In principle, this trend can be mathematically modelled and used as a predictive tool. However, a suitable physical model is required to account for the structure of the copolymer nano-objects. SAXS studies indicate structural order for the nano-objects at low copolymer concentration (Figure 3), while the electrophoretic data (Table S2) confirm that the nano-objects have anionic character. Thus, following Derjaguin, Landau, Verwey and Overbeek (DLVO) theory[50] the observed colloidal stability of these particles is consistent with a charge stabilization mechanism. In this context, it is noteworthy that the surface charge increases with the radius (Table S2). Considering that both parameters responsible for the colloidal stability[51] are related to each other, it is possible to hypothesize that the nano-objects become colloidally stable by acquiring a critical surface charge density. Since the MAA repeat units confer the surface charge, copolymer self-assembly most likely involves localization of this component at the particle surface. If this is correct, then reducing the MAA fraction in the copolymer chains leads to the formation of larger nano-objects in order to maintain a constant surface charge density. As an idealized approximation of the proposed scenario it could be assumed that *all* MAA units congregate at the particle surface. To test this assumption, the fraction of the nano-object surface covered by MAA residues was calculated for each particle from the known properties of the copolymer chains and the nano-objects they form.

Using a relatively simple geometric model and structural information obtained from SAXS, the location of the MAA units within the nano-object can be identified and used to relate the nano-object radius to the copolymer composition. First, various reasonable assumptions are made for this model: (1) the nano-objects are assumed to be perfect spheres; (2) all of the MAA segments are located on the

nano-object surface; (3) the total surface area covered by all the MAA residues is calculated using the volume occupied by one MAA unit, where each unit is represented by a cube and one face makes up a fraction of the nano-object surface.

The mole fraction of MAA residues in an individual copolymer chain is directly related to the mole fraction of MAA within a nano-object, which can be defined by the equation:

$$Mol.frac._{MAA} = \frac{N_{MAA,no}}{N_{MAA,no} + N_{BMA,no}} \quad (14)$$

where $N_{MAA,no}$ and $N_{BMA,no}$ are the mean number of MAA and BMA units per nano-object, respectively. These parameters can be obtained either from experiment using the copolymer composition or from the proposed model using the following equations:

$$N_{MAA,no} = \frac{4\pi R_s{}^2 \times SA_{frac}}{CS_{MAA}} \quad (15)$$

$$N_{BMA,no} = \frac{\frac{4}{3}\pi R_s{}^3 - \left(\frac{4\pi R_s{}^2 \times SA_{frac} \times V_{MAA}}{CS_{MAA}}\right)}{V_{BMA}} \quad (16)$$

where V_{MAA} = 121 Å^3 and V_{BMA} = 224 Å^3, calculated by the method described in the discussion following eq 7. CS_{MAA} is the approximate cross-sectional area of one MAA unit calculated from V_{MAA} ($= V_{MAA}^{2/3} \approx 24.5$ Å^2). SA_{frac} is the fraction of the nano-object surface covered by MAA residues. Equations 15 – 17 can be used to theoretically predict how the nano-object radius, R_s, is related to the mole fraction of MAA residues in the copolymer composition assuming that all these repeat units are located within the nano-object surface and given that SA_{frac}, which is proportional to the surface charge density, is a known constant (derived from electrophoretic data).

From the experimental data, larger nano-objects are formed as the MAA volume fraction of the copolymer is reduced (Figure 10). A similar dependence is also predicted by the structural model if it is

assumed that all MAA residues are located at the nano-objects surface and its surface fraction, SA_{frac}, is constant and independent of the particle size (Figure 10). The striking similarity between the experimental data and the theoretical prediction by this model suggests that most of the MAA units are indeed localized at the nano-objects surface. All the experimental data lie within a narrow interval of SA_{frac} values and approximately follow a curve corresponding to SA_{frac} = 0.30 (Figure 10). The discrepancies observed between the idealized model and the experimental results is likely to be related to the statistical nature of the copolymer chains. The average contour length of the mean sequence of BMA repeat unit is probably shorter than the particle diameter. As a result, some MAA units are surrounded by neighboring BMA units and hence may become 'trapped' within the particle cores. Thus, a more physically realistic structural model should have a core-shell morphology (or perhaps a gradient distribution of MAA repeat units) with a relatively high concentration of MAA units in the particle shell (surface) and a relatively low concentration of MAA units within the particle core. A similar model has been invoked in a recent work on self-assembly of a poly(methyl methacrylate-co-2-dimethyl aminoethyl methacrylate) random copolymer.[19] Nevertheless, the proposed idealized model suggests that the colloidal stability involves achieving a critical surface charge density that is mainly governed by the MAA content of the copolymer chains. This crude structural model can be used to estimate the dimensions of particles formed by the self-assembly of a series of amphiphilic statistical copolymers of variable MAA content. In principle, incorporating an additional parameter that accounts for the spatial distribution of MAA repeat units throughout an individual nano-object would improve the predictions of this model, but this is beyond the scope of this study.
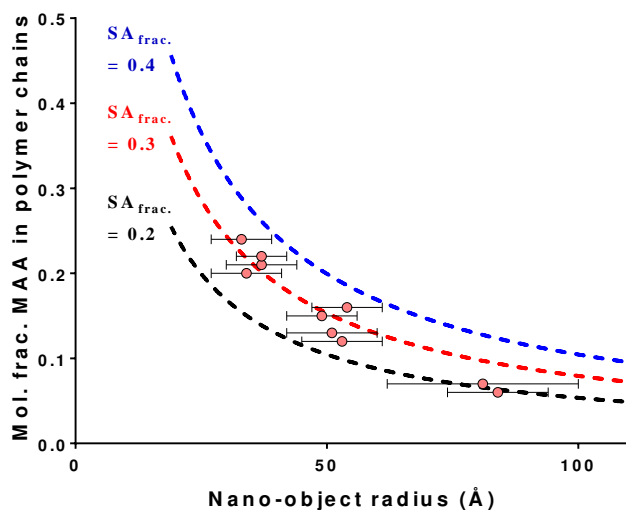
Figure 10. Relationship between the mole fraction of MAA segments in the copolymer chains and the corresponding nano-object radius formed in aqueous solution: experimental data (circles) and estimated values (dashed lines) using the model (eqs 14-16) when $SA_{frac.}$ = 0.40 (blue), 0.30 (red), and 0.20 (black).

CONCLUSIONS

A series of P(BMA-*stat*-MAA) statistical copolymers have been synthesized with various BMA/MAA compositions (77:23 – 93:7) and copolymer molecular weights (6 – 22 kDa) *via* RAFT solution copolymerization and compared to similar statistical copolymers prepared *via* monomer-starved conventional FRP. RAFT copolymerization produced low-dispersity copolymers ($M_w/M_n \approx$ 1.20), whereas FRP produced copolymers with somewhat higher dispersities ($M_w/M_n \approx$ 1.85). Kinetic analysis of the RAFT copolymerization found that both comonomers react at similar rates initially. However, the MAA conversion was lower than BMA towards the end of the copolymerization, leading to a short 'blocky' BMA-rich sequence towards the end of each copolymer chain. Conversely, FRP produced copolymers with an essentially random distribution of comonomer units.

SAXS studies of the effect of varying the IPA/water binary solvent composition on the morphology of the self-assembled structures in the presence of base (*ca*. pH 8) indicated that the copolymers are largely present as molecularly-dissolved Gaussian chains when the solvent is IPA-rich but self-assemble to form well-defined spherical nano-objects when the solvent composition becomes water-rich. Nano-object radii are inversely proportional to the MAA content of such copolymers but remain independent of molecular weight. At high copolymer concentrations and intermediate IPA/water solvent compositions, SAXS indicated the formation of relatively large objects. This is interpreted in terms of an inter-connected nano-object network created by the overlap of swollen nano-objects confined in space. These morphological insights correlate well with rheological measurements. At low copolymer concentrations, non-interacting spherical nano-objects are formed and the dispersions exhibit viscosities comparable to that of water. At high copolymer and IPA concentrations, when the dispersions become molecularly-dissolved copolymer chains, the solution viscosities are molecular weight-dependent, as expected. At intermediate copolymer and IPA concentrations, a pronounced maximum in solution viscosity is observed, which is consistent with the formation of the inter-connected nano-object network structures indicated by the SAXS data.

A relatively simple structural model involving just a form factor for spherical particles proved to be a good first approximation for the SAXS analysis of nano-objects formed by self-assembly of amphiphilic P(BMA-*stat*-MAA) statistical copolymers. This model has been refined by incorporating additional terms to account for fluctuating scattering length density associated with randomly-packed MAA and BMA repeat units, and scattering arising from a large inter-connected nano-object network. An appropriate structure factor has also been incorporated into this model to analyze the nano-object packing. This more sophisticated model provided good fits to all experimental SAXS patterns obtained for these copolymer dispersions, allowing determination of particle size, particle size distribution, the solvent concentration inside the particle cores and the mean molecule aggregation number.

Combined SAXS and electrophoretic measurements indicate that the nano-object size is directly related to the surface charge density and, therefore, the fraction of the nano-object surface covered by MAA. A new structural model assuming that the hydrophilic (MAA) units are localized at the particle surface and the hydrophobic (BMA) units mainly form the particle core has been proposed that is consistent with the experimental data and can be used as a first approximation to predict nano-object dimensions for aqueous dispersions of amphiphilic statistical copolymers.

ASSOCIATED CONTENT

Supporting Information. Representative curves of dynamic viscosity vs. angular frequency, table summarizing the reagent quantities required in the RAFT copolymerization, summary of copolymer characterization data, electrophoretic data, dependence of viscosity on sample composition and SAXS patterns with accompanying images of copolymer dispersions in the presence of added electrolyte.

AUTHOR INFORMATION

Corresponding Authors

*E-mail: o.mykhaylyk@sheffield.ac.uk, (O.O.M.)

*E-mail: s.g.spain@sheffield.ac.uk (S.G.S)

REFERENCES

(1)   Rösler, A.; Vandermeulen, G. W. M.; Klok, H. A. Advanced Drug Delivery Devices via Self-Assembly of Amphiphilic Block Copolymers. *Adv. Drug Deliv. Rev.* **2012**, *64*, 270–279.

(2)   Morishima, Y.; Nomura, S.; Ikeda, T.; Seki, M.; Kamachi, M. Characterization of Unimolecular Micelles of Random Copolymers of Sodium 2-(Acrylamido)-2-Methylpropanesulfonate and Methacrylamides Bearing Bulky Hydrophobic Substituents. *Macromolecules* **1995**, *28* (8), 2874–2881.

(3)   Li, L.; Raghupathi, K.; Song, C.; Prasad, P.; Thayumanavan, S. Self-Assembly of Random Copolymers. *Chem. Commun.* **2014**, *50* (88), 13417–13432.

(4)   Xu, R.; Winnik, M. A.; Hallett, F. R.; Riess, G.; Croucher, M. D. Light-Scattering Study of the Association Behavior of Styrene-Ethylene Oxide Block Copolymers in Aqueous Solution. *Macromolecules* **1991**, *24* (1), 87–93.

(5)   Wilhelm, M.; Zhao, C. Le; Wang, Y.; Xu, R.; Winnik, M. A.; Mura, J. L.; Riess, G.; Croucher, M. D. Poly(styrene-Ethylene Oxide) Block Copolymer Micelle Formation in Water: A Fluorescence Probe Study. *Macromolecules* **1991**, *24* (5), 1033–1040.

(6)   Prochazka, K.; Kiserow, D.; Ramireddy, C.; Munk, P.; Webber, S. E.; Tuzar, Z. Time-Resolved Fluorescence Studies of the Chain Dynamics of Naphthalene-Labeled Polystyrene-Block-Poly(methacrylic Acid) Micelles in Aqueous Media. *Macromolecules* **1992**, *25* (1), 454–460.

(7)   Astafieva, I.; Zhong, X. F.; Eisenberg, A. Critical Micellization Phenomena in Block

Polyelectrolyte Solutions. *Macromolecules* **1993**, *26*, 7339.

(8)   Qin, A.; Tian, M.; Ramireddy, C.; Webber, S. E.; Munk, P.; Tuzar, Z. Polystyrene–

      Poly(methacrylic Acid) Block Copolymer Micelles. *Macromolecules* **1994**, *27* (1), 120–126.

(9)   Guo, M.; Pitet, L. M.; Wyss, H. M.; Vos, M.; Dankers, P. Y. W.; Meijer, E. W. Tough Stimuli-

      Responsive Supramolecular Hydrogels with Hydrogen-Bonding Network Junctions. *J. Am. Chem.*

      Soc. **2014**, *136* (19), 6969–6977.

(10) Huo, M.; Yuan, J.; Tao, L.; Wei, Y. Redox-Responsive Polymers for Drug Delivery: From

      Molecular Design to Applications. *Polym. Chem.* **2014**, *5* (5), 1519.

(11) Schattling, P.; Jochum, F. D.; Theato, P. Multi-Stimuli Responsive Polymers – the All-in-One

      Talents. *Polym. Chem.* **2014**, *5* (1), 25–36.

(12) Sun, Y.; Wang, Z.; Li, Y.; Zhang, Z.; Zhang, W.; Pan, X.; Zhou, N.; Zhu, X. Photoresponsive

      Amphiphilic Macrocycles Containing Main-Chain Azobenzene Polymers. *Macromol. Rapid*

      Commun. **2015**, 1341–1347.

(13) Blanazs, A.; Madsen, J.; Battaglia, G.; Ryan, A. J.; Armes, S. P. Mechanistic Insights for Block

      Copolymer Morphologies: How Do Worms Form Vesicles? *J. Am. Chem. Soc.* **2011**, *133*,

      16581–16587.

(14) Blanazs, A.; Ryan, A. J.; Armes, S. P. Predictive Phase Diagrams for RAFT Aqueous Dispersion

      Polymerization: Effect of Block Copolymer Composition, Molecular Weight, and Copolymer

      Concentration. *Macromolecules* **2012**, *45*, 5099–5107.

(15) Mable, C. J.; Gibson, R. R.; Prevost, S.; McKenzie, B. E.; Mykhaylyk, O. O.; Armes, S. P.

      Loading of Silica Nanoparticles in Block Copolymer Vesicles during Polymerization-Induced

      Self-Assembly: Encapsulation Efficiency and Thermally Triggered Release. *J. Am. Chem. Soc.*

      2015, *137* (51), 16098–16108.

(16) Blanazs, A.; Armes, S. P.; Ryan, A. J. Self-Assembled Block Copolymer Aggregates: From Micelles to Vesicles and Their Biological Applications. *Macromol. Rapid Commun.* **2009**, *30* (4–5), 267–277.

(17) Scheler, U. *Handbook of Polyelectrolytes and Their Application, Vol. 2*; American Scientific Publishers: California, 2002.

(18) Hu, Y.; Armentrout, R. S.; McCormick, C. L. Water Soluble Polymers. 75. Responsive Microdomains in Labeled N-Octylamide-Substituted Poly(sodium Maleate-Alt-Ethyl Vinyl Ether): Transient Fluorescence and Time-Resolved Fluorescence Anisotropy Studies. *Macromolecules* **1997**, *30*, 3538–3546.

(19) Pegg, J. C.; Czajka, A.; Hill, C.; James, C.; Peach, J.; Rogers, S. E.; Eastoe, J. Alternative Route to Nanoscale Aggregates with a pH-Responsive Random Copolymer. *Langmuir* **2017**, *33* (10), 2628–2638.

(20) Hales, K.; Pochan, D. J. Using Polyelectrolyte Block Copolymers to Tune Nanostructure Assembly. *Curr. Opin. Colloid Interface Sci.* **2006**, *11* (6), 330–336.

(21) Hirai, Y.; Terashima, T.; Takenaka, M.; Sawamoto, M. Precision Self-Assembly of Amphiphilic Random Copolymers into Uniform and Self-Sorting Nanocompartments in Water. *Macromolecules* **2016**, *49* (14), 5084–5091.

(22) Chang, Y.; McCormick, C. L. Water-Soluble Copolymers. 49. Effect of the Distribution of the Hydrophobic Cationic Monomer Dimethyldodecyl(2-acrylamidoethy1)ammonium Bromide on the Solution Behavior of Associating Acrylamide Copolymers. *Macromolecules* **1993**, *26*, 6121.

(23) Hashidzume, A.; Kawaguchi, A.; Tagawa, A.; Hyoda, K.; Sato, T. Synthesis and Structural Analysis of Self-Associating Amphiphilic Statistical Copolymers in Aqueous Media. *Macromolecules* **2006**, *39* (3), 1135–1143.

(24)   Kawata, T.; Hashidzume, A.; Sato, T. Micellar Structure of Amphiphilic Statistical Copolymers Bearing Dodecyl Hydrophobes in Aqueous Media. *Macromolecules* **2007**, *40* (4), 1174–1180.

(25)   Zhu, X.; Liu, M. Self-Assembly and Morphology Control of New L -Glutamic Acid-Based Amphiphilic Random Copolymers: Giant Vesicles, Vesicles, Spheres, and Honeycomb Film. *Langmuir* **2011**, *27* (21), 12844–12850.

(26)   Guo, P.; Guan, W.; Liang, L.; Yao, P. Self-Assembly of pH-Sensitive Random Copolymers: Poly(styrene-Co-4-Vinylpyridine). *J. Colloid Interface Sci.* **2008**, *323* (2), 229–234.

(27)   Liu, X.; Kim, J.-S.; Wu, J.; Eisenberg, A. Bowl-Shaped Aggregates from the Self-Assembly of an Amphiphilic Random Copolymer of Poly(styrene- Co -Methacrylic Acid). *Macromolecules* **2005**, *38* (16), 6749–6751.

(28)   Tian, F.; Yu, Y.; Wang, C.; Yang, S. Consecutive Morphological Transitions in Nanoaggregates Assembled from Amphiphilic Random Copolymer via Water-Driven Micellization and Light-Triggered Dissociation. *Macromolecules* **2008**, *41* (10), 3585–3588.

(29)   Wu, X.; Qiao, Y.; Yang, H.; Wang, J. Self-Assembly of a Series of Random Copolymers Bearing Amphiphilic Side Chains. *J. Colloid Interface Sci.* **2010**, *349* (2), 560–564.

(30)   Ilhan, F.; Galow, T. H.; Gray, M.; Clavier, G.; Rotello, V. M. Giant Vesicle Formation through Self-Assembly of Complementary Random Copolymers [10]. *J. Am. Chem. Soc.* **2000**, *122* (24), 5895–5896.

(31)   Riemer, S.; Prévost, S.; Dzionara, M.; Appavou, M.-S.; Schweins, R.; Gradzielski, M. Aggregation Behaviour of Hydrophobically Modified Polyacrylate – Variation of Alkyl Chain Length. *Polymer (Guildf)*. **2015**, *70*, 194–206.

(32)   Semsarilar, M.; Ladmiral, V.; Blanazs, A.; Armes, S. P. Poly(methacrylic Acid)-Based AB and ABC Block Copolymer Nano-Objects Prepared via RAFT Alcoholic Dispersion Polymerization.

Polym. Chem. **2014**, *5* (10), 3466–3475.

(33)   Ilavsky, J. Nika: Software for Two-Dimensional Data Reduction. *J. Appl. Crystallogr.* **2012**, *45* (2), 324–328.

(34)   Ilavsky, J.; Jemian, P. R. Irena: Tool Suite for Modeling and Analysis of Small-Angle Scattering. *J. Appl. Crystallogr.* **2009**, *42* (2), 347–353.

(35)   Cockram, A. A.; Neal, T. J.; Derry, M. J.; Mykhaylyk, O. O.; Williams, N. S. J.; Murray, M. W.; Emmett, S. N.; Armes, S. P. Effect of Monomer Solubility on the Evolution of Copolymer Morphology during Polymerization-Induced Self-Assembly in Aqueous Solution. *Macromolecules* **2017**, *50* (3), 796–802.

(36)   Chiefari, J.; Chong, Y. K. (Bill); Ercole, F.; Krstina, J.; Jeffery, J.; Le, T. P. T.; Mayadunne, R. T. A.; Meijs, G. F.; Moad, C. L.; Moad, G.; Rizzardo, E.; Thang, S. H. Living Free-Radical Polymerization by Reversible Addition−Fragmentation Chain Transfer: The RAFT Process. *Macromolecules* **1998**, *31* (16), 5559–5562.

(37)   Pedersen, J. S.; Gerstenberg, M. C. Scattering Form Factor of Block Copolymer Micelles. *Macromolecules* **1996**, *29* (4), 1363–1365.

(38)   Percus, J. K.; Yevick, G. J. Analysis of Classical Statistical Mechanics by Means of Collective Coordinates. *Phys. Rev.* **1958**, *110* (1), 1–13.

(39)   Hayter, J. B.; Penfold, J. An Analytic Structure Factor for Macroion Solutions. *Mol. Phys.* **1981**, *42*, 109–118.

(40)   Delgado, A. V.; González-Caballero, F.; Hunter, R. J.; Koopal, L. K.; Lyklema, J. Measurement and Interpretation of Electrokinetic Phenomena (IUPAC Technical Report). *Pure Appl. Chem.* **2005**, *77* (10), 1753–1805.

(41)   Hsu, M. F.; Dufresne, E. R.; Weitz, D. A. Charge Stabilization in Nonpolar Solvents. *Langmuir* **2005**, *21* (11), 4881–4887.

(42)   Pedersen, J. S. Form Factors of Block Copolymer Micelles with Spherical, Ellipsoidal and Cylindrical Cores. *J. Appl. Crystallogr.* **2000**, *33* (3 I), 637–640.

(43)   Pedersen, J. S.; Hamley, I. W.; Ryu, C. Y.; Lodge, T. P. Contrast Variation Small-Angle Neutron Scattering Study of the Structure of Block Copolymer Micelles in a Slightly Selective Solvent at Semidilute Concentrations. *Macromolecules* **2000**, *33* (2), 542–550.

(44)   Doi, M.; Edwards, S. F. *The Theory of Polymer Dynamics*; Claredon Press: Oxford, 1986.

(45)   Beaucage, G.; Schaefer, D. W. W. Structural Studies of Complex Systems Using Small-Angle Scattering: A Unified Guinier/power-Law Approach. *J. Non. Cryst. Solids* **1994**, *172–174*, 797–805.

(46)   Beaucage, G. Approximations Leading to a Unified Exponential/Power-Law Approach to Small-Angle Scattering. *J. Appl. Crystallogr.* **1995**, *28* (6), 717–728.

(47)   Beaucage, G. Small-Angle Scattering from Polymeric Mass Fractals of Arbitrary Mass-Fractal Dimension. *J. Appl. Crystallogr.* **1996**, *29* (2), 134–146.

(48)   Lee, C.; Jeoung, E.; Lee, I. Effect of Mixtures of Water and Organic Solvents on the Acidities of 5-Membered Heteroaromatic Carboxylic Acids. *Journal of Heterocyclic Chemistry*. 2000, pp 159–166.

(49)   Willenbacher, N.; Georgieva, K. Rheology of Disperse Systems. In *Product Design and Engineering: Formulation of Gels and Pastes*; Brockel, U., Meier, W., Wgner, G., Eds.; Wiley-VCH Verlag GmbH & Co. KGaA.: Weinheim, 2013; pp 7–49.

(50)   Hunter, R. J. *Foundations of Colloid Science*, 2nd ed.; Oxford University Press: New York, 2000.

(51) Hidalgo-Álvarez, R.; Martín, A.; Fernández, A.; Bastos, D.; Martínez, F.; De Las Nieves, F. J. Electrokinetic Properties, Colloidal Stability and Aggregation Kinetics of Polymer Colloids. *Adv. Colloid Interface Sci.* **1996**, *67*, 1–118.

43

Self-assembly of amphiphilic statistical copolymers and their aqueous rheological properties

Thomas J. Neal, Deborah L. Beattie, Sarah J. Byard, Gregory N. Smith, Martin W. Murray, Neal S. J. Williams, Simon N. Emmett, Steven P. Armes, Sebastian G. Spain, Oleksandr O. Mykhaylyk